

Unsteady Hybrid Navier-Stokes/Vortex Model Applied to Wind Turbine Aerodynamics under Yaw Conditions

Kensuke Suzuki* and Jean-Jacques Chattot*
Corresponding author: kensuzuki@ucdavis.edu

* University of California, Davis, USA.

Abstract: A new analysis tool, an unsteady Hybrid Navier-Stokes/Vortex Model, for a horizontal axis wind turbine (HAWT) in yawed flow is presented, and its convergence and low cost computational performance are demonstrated. The unsteady hybrid model is applied to the NREL Unsteady Aerodynamic Experiment (UAE) Phase VI rotor at 10 and 20 degrees of yaw and the global and local results are compared with the Vortex Line Method (VLM) and experiments. The unsteady motion of the blade tip vortices in yawed flow is visualized. A 10 % backward swept rotor is also analyzed in yawed flow as an example of the new tool. A new acceleration technique for prescribed wake model is introduced, and its successful result is presented.

Keywords: Unsteady flow, Hybrid model, Wind turbine aerodynamics, Dual time steps, Acceleration technique.

1 Introduction

The Hybrid Navier-Stokes/Vortex Model was developed by Schmitz and Chattot and applied to the UAE Phase VI experiment for steady flow at zero yaw [1]. The results showed that the model improved the global force predictions over wind speeds from fully attached flow to separated flows, as well as the agreement of the local pressure distributions with the experiments, compared to the results from participants of the NASA Ames blind comparison workshop [2]. In earlier work, the steady hybrid model was applied to an optimum wind turbine blade [3], and a 10 % backward swept blade [4], to investigate these designs for HAWT. An unsteady VLM code has been developed for yawed flow, blade tower interaction, earth boundary layer effects and wind gusts, and has been validated with the UAE experiment and other reference data [5, 6]. The unsteady VLM was used by GE, coupled with ADAMS/AeroDyn, to study aeroelastic effects due to blade sweep and winglets [7]. In this work, the unsteady helicoidal vortex model is coupled with the unsteady Navier-Stokes (NS) solver, CFX V12.0. The unsteady hybrid model is applied to the NREL UAE Phase VI rotors under 10 and 20 degrees of yaw and the local and global results are compared with the results of VLM and experimental data. The computational performance is contrasted with results of unsteady Euler and Navier-Stokes computations as standard references. A 10 % backward swept “NREL blade” is analyzed under 10 degrees of yaw as an example of the new tool, and the blade tip vortices are visualized.

2 Unsteady hybrid method

2.1 Unsteady helicoidal vortex model

The vortex sheets behind a wind turbine rotor are modeled as perfect helices, generated by the rotation of the lifting line segment around the axis of the rotor and its translation towards the Trefftz plane (see Fig. 1). The translation velocity is modeled to vary linearly, from the rotor plane to some location, typically three turns of the helix from the rotor plane, and then to remains constant to the Trefftz plane [8].

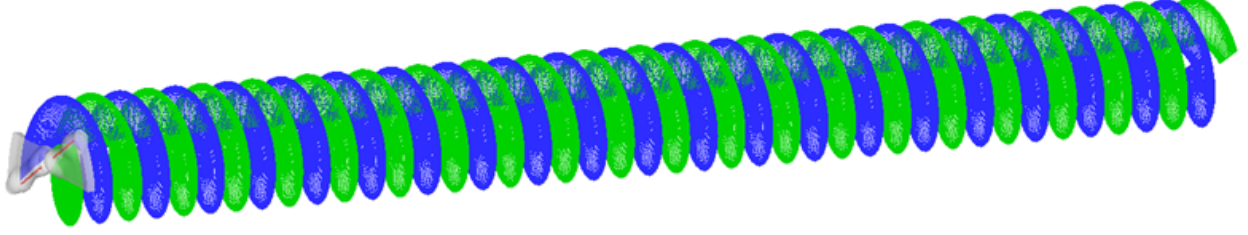


Figure 1: Lifting lines and vortex sheets with outline of Navier-Stokes zones

Let $\vec{V}_{wind} = (U, 0, 0)$ be the incoming wind velocity vector. The average axial induced velocity at the rotor " u ", is estimated by a "wake equilibrium condition" such that the power, P , absorbed (negative) by the rotor matches the power deficit in the far wake obtained from the actuator disk theory:

$$P = \tau\Omega = 2\pi\rho U^3 R^2(1+u)^2u \quad (1)$$

where ρ , R , Ω and τ represent the density of air, rotor radius, the angular velocity and the torque. Introducing the advance ratio $adv = U/\Omega R$, the torque coefficient C_τ and the power coefficient C_p , the condition can be written as a cubic equation for " u ", with the target power coefficient as input data, and it is solved iteratively using Newton's method.

$$-4(1+u)^2u = \frac{C_\tau}{adv} = C_p \quad (2)$$

The computational mesh on the vortex sheet is constructed as follows (see Fig. 2). Let x_i , y_i and z_i represent the tip vortex of blade1. The grid in the x -axis direction is stretched from the lifting line to a specified location $x_{str} \approx 1$ using a stretching parameter, $s > 1$, where the coordinates are normalized by the blade radius.

$$x_i = x_{i-1} + dx_{i-1}, \quad dx_i = s dx_{i-1}, \quad i = 2, \dots, i_{str} \quad (3)$$

After $x = x_{str}$, a uniform mesh spacing is used to the Trefftz plane $x_{ix} \approx 20$.

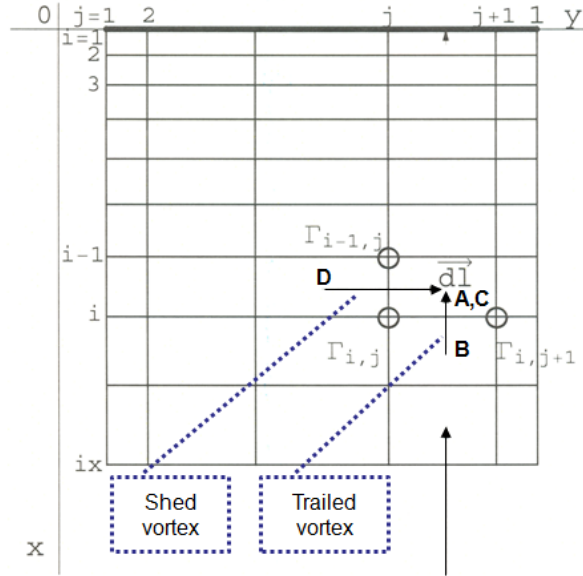


Figure 2: Schematic representation of a vortex sheet

The advance ratio, adv , which is the inverse of the tip speed ratio, TSR , varies from $adv_1 = (U + u)/\Omega R$ to $adv_{ix} = (U + 2u)/\Omega R$, and the y_i and z_i are defined using

$$y_i = \cos\left(\frac{x_i}{adv_i}\right), \quad z_i = \sin\left(\frac{x_i}{adv_i}\right) \quad (4)$$

In the y -direction, the mesh has a cosine distribution:

$$y_j = y_0 + \frac{1}{2}(1 - y_0)\cos\theta_j, \quad \theta_j = \frac{j-1}{j_x-1}\pi, \quad j = 1, \dots, j_x \quad (5)$$

The circulation, $\Gamma_{i,j}$, on the lifting line and the vortex sheet is defined at the grid points of the lattice, and the trailed and shed vortices are located between the mesh lines. The trailed vortices are located at

$$\eta_j = y_0 + \frac{1}{2}(1 - y_0)\cos\theta_j, \quad \theta_j = \frac{2j-1}{2(j_x-1)}\pi, \quad j = 1, \dots, j_x - 1 \quad (6)$$

The strength of the trailed vorticity elements is given in terms of the difference in circulation:

$$\Delta\Gamma_{i,j} = \Gamma_{i,j+1} - \Gamma_{i,j} \quad (7)$$

The strength of the shed vorticity elements is given by:

$$\Delta\Gamma_{i,j} = \Gamma_{i,j} - \Gamma_{i-1,j} \quad (8)$$

The bound vorticity of the lifting line is given by:

$$\Delta\Gamma_{1,j} = \Gamma_{1,j} \quad (9)$$

The component of the small element of the trailed vortex, $d\vec{l}_{AB}$ in the figure is:

$$\begin{aligned} \vec{l}_A &= \frac{1}{2} \begin{pmatrix} x_i + x_{i-1} \\ \eta_j \cos \frac{x_i}{adv_i} + \eta_j \cos \frac{x_{i-1}}{adv_{i-1}} \\ \eta_j \sin \frac{x_i}{adv_i} + \eta_j \sin \frac{x_{i-1}}{adv_{i-1}} \end{pmatrix}, \\ \vec{l}_B &= \frac{1}{2} \begin{pmatrix} x_i + x_{i+1} \\ \eta_j \cos \frac{x_i}{adv_i} + \eta_j \cos \frac{x_{i+1}}{adv_{i+1}} \\ \eta_j \sin \frac{x_i}{adv_i} + \eta_j \sin \frac{x_{i+1}}{adv_{i+1}} \end{pmatrix}, \\ \vec{dl} &= (\vec{l}_A - \vec{l}_B)^T \\ &= \left\{ -\frac{1}{2}(x_{i+1} - x_{i-1}), -\frac{1}{2}\eta_j(y_{i+1} - y_{i-1}), -\frac{1}{2}\eta_j(z_{i+1} - z_{i-1}) \right\} \end{aligned} \quad (10)$$

The trailed element which is closest to the lifting line is treated with half cell size at $\frac{1}{2}(x_1 + x_2)$, and the element at the Trefftz plane is extended from infinity to $\frac{1}{2}(x_{i-1} + x_{i+1})$, as seen in Fig. 2. The main difference for the unsteady model compared to the steady one is that the circulation generated at the blade sections is time dependent and varies along the vortex filament. Hence the shed vorticity, $\Gamma_{i,j} - \Gamma_{i-1,j}$ is not zero. A small element of the shed vorticity, $d\vec{l}_{CD}$ is:

$$\begin{aligned} \vec{l}_D &= \vec{l}_A, \\ \vec{l}_C &= \frac{1}{2} \begin{pmatrix} x_i + x_{i-1} \\ \eta_{j-1} \cos \frac{x_i}{adv_i} + \eta_{j-1} \cos \frac{x_{i-1}}{adv_{i-1}} \\ \eta_{j-1} \sin \frac{x_i}{adv_i} + \eta_{j-1} \sin \frac{x_{i-1}}{adv_{i-1}} \end{pmatrix}, \\ \vec{dl} &= (\vec{l}_D - \vec{l}_C)^T \\ &= \left\{ 0, -\frac{1}{2}(y_i + y_{i-1})(\eta_j - \eta_{j-1}), -\frac{1}{2}(z_i + z_{i-1})(\eta_j - \eta_{j-1}) \right\} \end{aligned} \quad (11)$$

The bound vortex elements on the lifting line are defined at the grid points and have the components

$$\vec{dl} = \{0, \eta_j - \eta_{j-1}, 0\}, \quad j = 2, \dots, j_x - 1 \quad (12)$$

The bound circulations on the lifting line are updated from the Navier-Stokes solution during the coupling process. The circulation on the vortex sheets is convected along the wake with the average axial velocity of the Trefftz plane, $1 + 2u$, where $u < 0$ is the axial inductance at the rotor blade.

$$\frac{\partial \Gamma}{\partial t} + (1 + 2u) \frac{\partial \Gamma}{\partial x} = 0 \quad (13)$$

For this convection equation, a two point semi-implicit scheme is used [5, 8, 9]

$$\begin{aligned} & \theta \frac{\Gamma_i^{n+\frac{\nu}{\nu+1}} - \Gamma_i^n}{\Delta t} + (1 - \theta) \frac{\Gamma_{i-1}^{n+\frac{\nu}{\nu+1}} - \Gamma_{i-1}^n}{\Delta t} \\ + & \theta (1 + 2u) \frac{\Gamma_i^{n+\frac{\nu}{\nu+1}} - \Gamma_{i-1}^{n+\frac{\nu}{\nu+1}}}{x_i - x_{i-1}} + (1 - \theta) (1 + 2u) \frac{\Gamma_i^n - \Gamma_{i-1}^n}{x_i - x_{i-1}} = 0 \end{aligned} \quad (14)$$

When the parameter $\theta = 1/2$, the scheme reduces to the Crank-Nicolson scheme. For $\theta \geq 1/2$, the scheme is unconditionally stable. The symbol ν represents the inner iteration loop within one time step. The convection equation with the proposed scheme and mesh spacing converged in 2-3 sub-iterations for all test cases in this study.

2.2 Navier-Stokes solver

In analyses under yaw or tower interaction, each blade exhibits different conditions in time and space; hence, both blades must be analyzed simultaneously. Fig. 3 (a) shows the coordinate system with incoming velocity components under yaw angle β . As seen in Fig. 1 and Fig. 3, the Navier-Stokes computational domain size of the hybrid method extends a few chords about the blade. CFX has the capability of simulating isolated zones, and it is possible to simulate multiple blades with the duplication of a single blade mesh. The boundary condition at the outer surface of the Navier-Stokes zones is set by the velocity component.

$$\vec{V}_c = \vec{V}_{wind} + \vec{V}_{rot} + \vec{V}_{ind} \quad (15)$$

where, $\vec{V}_{wind} = (U \cos \beta, U \sin \beta, 0)$ is the incoming wind velocity, \vec{V}_{rot} is the blade rotation entrainment velocity and \vec{V}_{ind} is the induced velocity, the perturbation due to bound vortices and shed and trailed vortices. The induced velocity of the small element at control point c on the outer boundary surface of the Navier-Stokes zone, is calculated with the Biot-Savart law

$$d\vec{V}_{i,j,c} = \frac{\Delta \Gamma_{i,j}}{4\pi} \frac{d\vec{l} \times \vec{r}_{i,j,c}}{|\vec{r}_{i,j,c}|^3} \quad (16)$$

Fig. 3 (b) shows the three components of the perturbation velocity induced by the selected filaments. The induced velocity components are calculated as

$$\begin{aligned} u'_{c,1} &= \sum_{i=1}^{ix} \sum_{j=1}^{jx-1} (\Gamma_{i,j+1,1} - \Gamma_{i,j,1}) a_{i,j,c,1} + \sum_{i=1}^{ix} \sum_{j=1}^{jx-1} (\Gamma_{i,j+1,2} - \Gamma_{i,j,2}) a_{i,j,c,2} \\ &+ \sum_{i=1}^{ix} \sum_{j=2}^{jx-1} (\Gamma_{i+1,j,1} - \Gamma_{i,j,1}) a_{i,j,c,3} + \sum_{i=1}^{ix} \sum_{j=2}^{jx-1} (\Gamma_{i+1,j,2} - \Gamma_{i,j,2}) a_{i,j,c,4} \\ &+ \sum_{j=2}^{jx-1} \Gamma_{1,j,1} \tilde{a}_{j,c,1} + \sum_{j=2}^{jx-1} \Gamma_{1,j,2} \tilde{a}_{j,c,2} \end{aligned} \quad (17)$$

where the first two terms correspond to the influence of the trailed vortices of the vortex sheets 1 and 2 on NS zone 1; the next two terms are the contributions of the shed vorticity; and the last two terms correspond to the influence of the lifting lines 1 and 2. The influence coefficient from the trailed vorticity components

at control point c , located at (x_c, y_c, z_c) , is

$$a_{i,j,c} = -\frac{1}{4\pi} \frac{(z_c - z_{ij}) dy_{ij} - (y_c - y_{ij}) dz_{ij}}{\left[(x_c - x_i)^2 + (y_c - y_{ij})^2 + (z_c - z_{ij})^2 \right]^{\frac{3}{2}}} \quad (18)$$

Similarly, the $v_{c,1}$ and $w_{c,1}$ components are stored in arrays $b_{i,j,c,n}$ and $c_{i,j,c,n}$, $n = 1, \dots, 4$, and are found by cyclic permutation;

$$\begin{aligned} (z_c - z_{ij}) &\rightarrow (x_c - x_i), & (y_c - y_{ij}) &\rightarrow (z_c - z_{ij}), & (x_c - x_i) &\rightarrow (y_c - y_{ij}) \\ dy_{ij} &\rightarrow dz_{ij}, & dz_{ij} &\rightarrow dx_i, & dx_i &\rightarrow dy_{ij} \end{aligned} \quad (19)$$

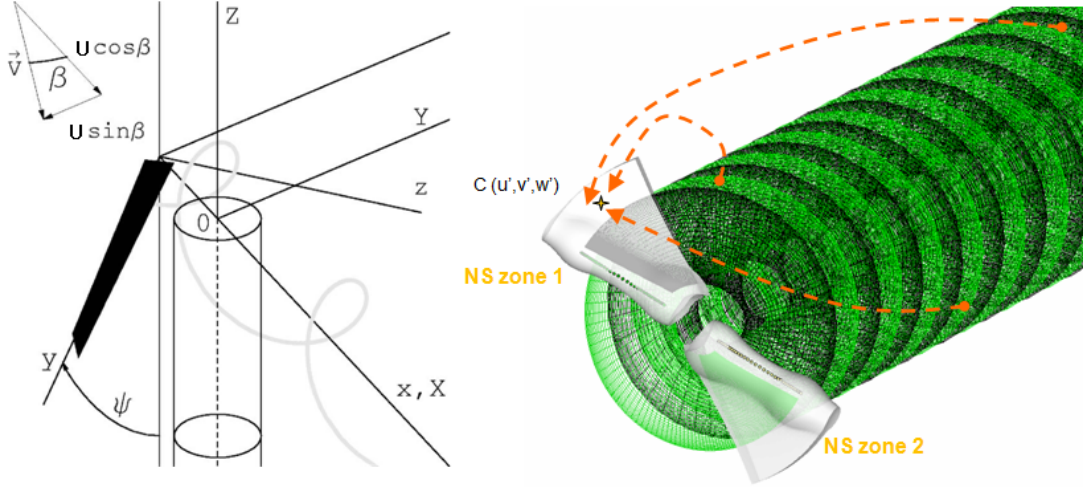


Figure 3: (a) Sketch of the rotor, tower, and coordinate system (left); (b) Induced velocity from selected filaments of the vortex sheets and a filament from blade 2 at control point c (right)

The velocity components obtained by combining the incoming velocity, the entrainment velocity due to the rotating frame and the induced velocity are used as Dirichlet boundary condition for the NS outer boundaries.

$$\begin{aligned} u_c &= U \cos \beta + u' \\ v_c &= U \sin \beta \sin \Psi - z \Omega + v' \\ w_c &= -U \sin \beta \cos \Psi + y \Omega + w' \end{aligned} \quad (20)$$

The bound circulation is calculated from the blade surface pressure solution using Kutta-Joukowski lift theorem. In this study, as a first order approximation, the circulation is convected on the base helix (in Fig. 1), not the actual helix displaced or distorted by yaw. With this simplification, the same influence coefficients can be used for blade 2 by symmetry in the geometry of the vortex sheets, i.e. the influence coefficient from blade 2 on zone 1 is equal to that from blade 1 on zone 2. With this approach, as yaw increases, the approximation associated with the base helix will introduce inaccuracies, but good predictions can still be obtained for yaw angles up to 20 or 30 degrees.

2.3 Dual time step

During the coupling process, different solvers that share the same physical transient boundary conditions generate solutions that independently satisfy each governing set of equations, but may not be consistent with the physics. Sub-iterations are performed until the solutions are considered to be physically consistent. In this study, the time dependent bound circulation along the blade span is chosen for the determination of the convergence of the coupled solutions for a time step. The sub-iteration process within a time step is reviewed by D. A. Caughey in the concept of temporal sub-iteration (or dual time stepping) [10].

3 UAE S Sequence Analysis

3.1 Mesh systems of the hybrid method

Mesh systems of the hybrid method are shown in Fig. 4.

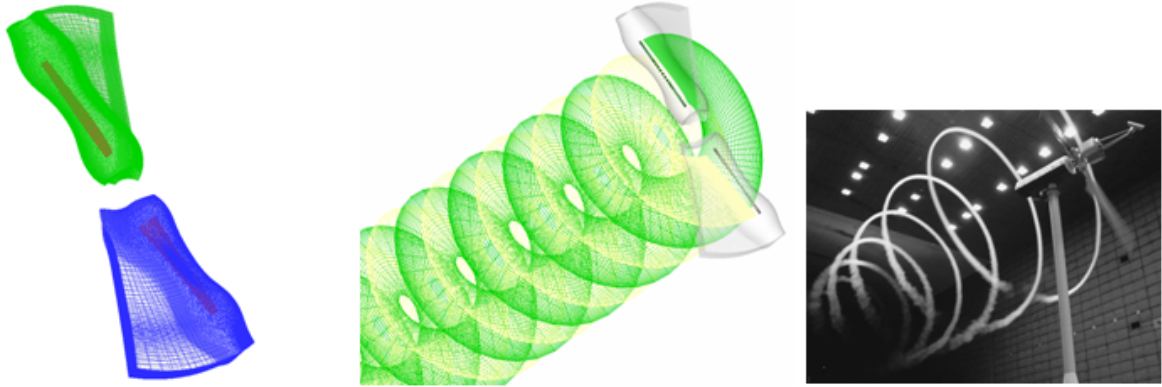


Figure 4: (a) Mesh system for the NS zone (left); (b) for vortex method, lifting lines and helicoidal vortex sheets (middle); (c) NREL rotor with tip vortex visualization (right)(Fingersh, 2001 [11])

Fig. 4 (a) shows a computational mesh for the NS solver. Fig. (b) shows the two vortex lattices and the lifting lines for the unsteady wake model superimposed upon the outline of the Navier-Stokes zone. Fig. 4 (c) is a picture of NREL blade with visualization of the tip vortex.

3.2 Convergence history

In the unsteady hybrid method the outer boundary velocity distribution is updated at every sub-iteration within a time step. Certain requirements must be met in order for the coupled solution to be accurate. The first requirement is that residuals of the time dependent governing equations be converged. The second requirement is the matching of the bound circulation for both the NS equations and the convection equation. Fig. 5 shows the convergence history of the RMS (the root mean square) normalized values of the residuals for 10 cycles, and shows that the values change periodically while staying below a tolerance of $1e-4$. Note that the 20 degree yaw case yields larger residuals.

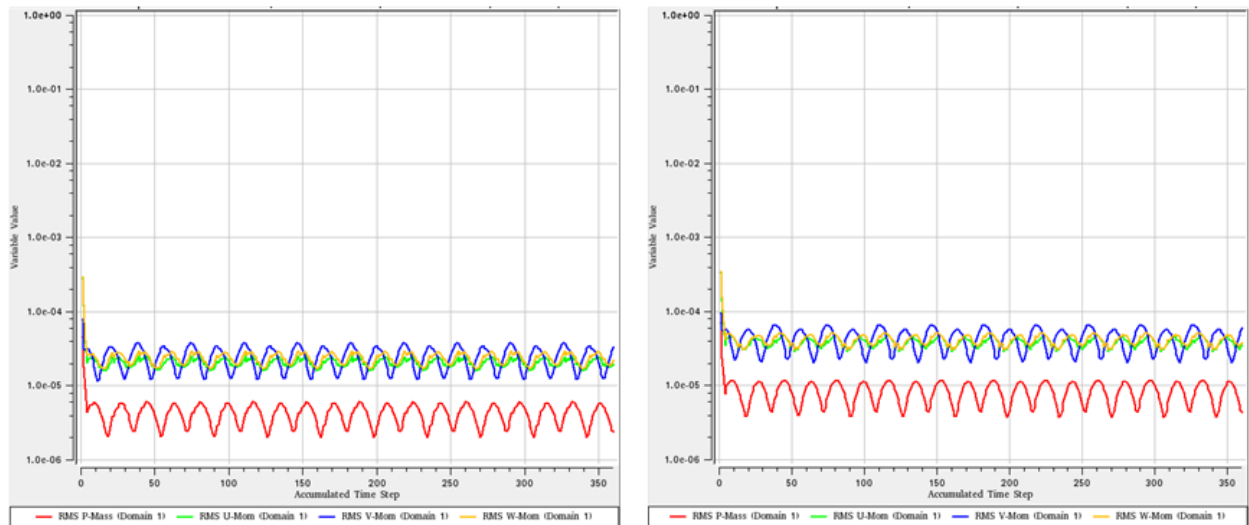


Figure 5: (a) The residual monitor at $V_{wind}=7$ m/s, 10 deg. of yaw, (left); (b) 20 deg. of yaw (right)

Fig. 6 shows the convergence history of the maximum correction of the bound circulation for 10th cycles under the 20 degrees of yaw condition. The values of the 3rd temporal sub-iteration are illustrated with circle markers; the coupling converges in 3 sub-iterations for both 10 and 20 degrees of yaw. Fig. 7 represents the power monitor window for blade 1, blade 2 and their summation as total power. In this test, 10 cycles of simulation were performed for the solution to become essentially periodic as seen from the power output monitor.

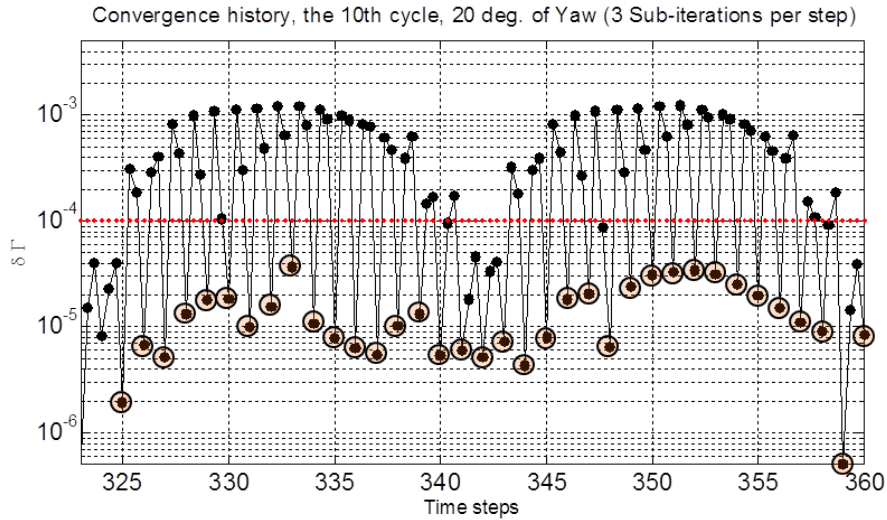


Figure 6: A detail of the maximum correction of the bound circulation for the 10th cycle under 20 degrees of yaw

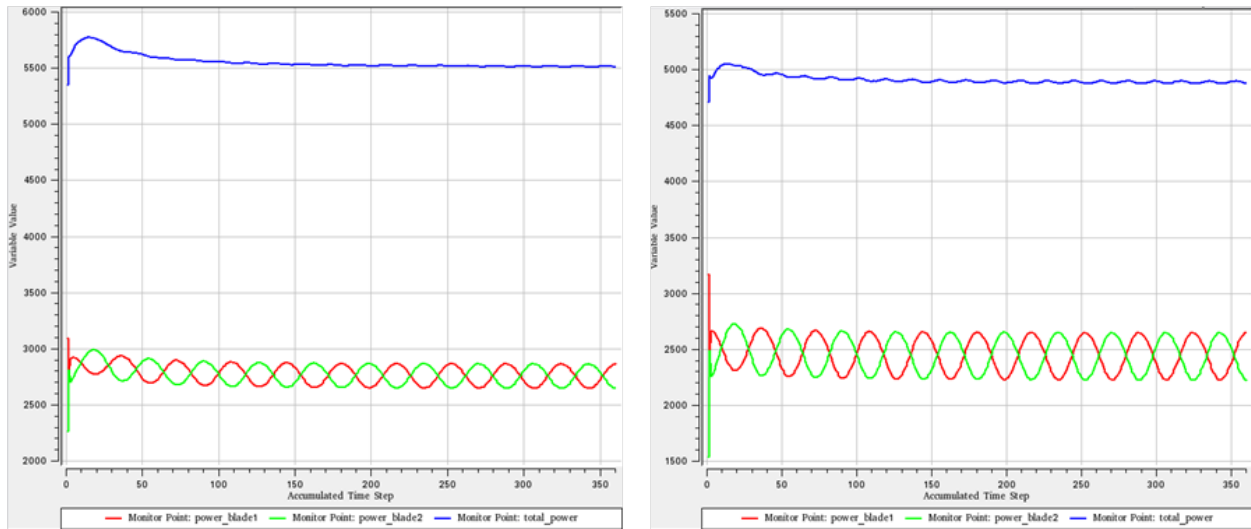


Figure 7: (a) The power monitor for blade 1, blade 2 and the total power under 10 degrees of yaw (left); (b) 20 degrees of yaw (right)

3.3 Results

Fig. 8 shows a comparison of the power output data with VLM and the NREL experimental data. The average power is summarized in Table 1. For an appropriate comparison, it must be remembered that, for both the VLM and Hybrid methods, the blade tower interaction was not modeled in this study.

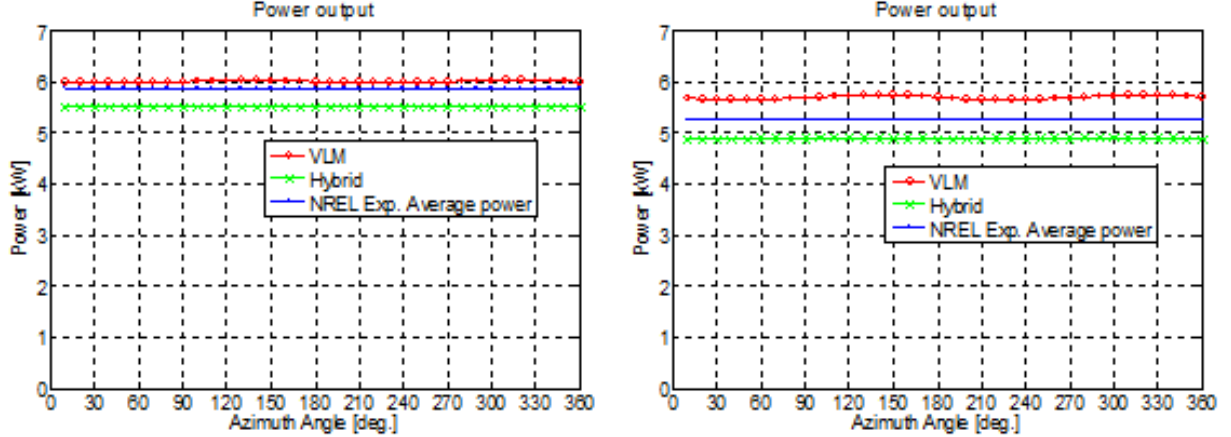


Figure 8: (a) Comparison of power output for NREL experiment and VLM under 10 degrees of yaw (left); (b) under 20 degrees of yaw

Average Power [kW], % of experiment in ()			
Yaw angle [deg.]	UAE Experiment	VLM	Hybrid
10	5.87	6.01 (+2.3%)	5.51 (-6.5%)
20	5.26	5.70 (+7.7%)	4.89 (-7.7%)

Table 1: Average power at $V_{wind}=7$ m/s, 10 and 20 degrees of yaw

Fig. 9 shows the comparisons of the bound circulation with VLM results at blade position downward (blade 1) and upward (blade 2), in which r corresponds to the y coordinate in Fig. 3 (a).

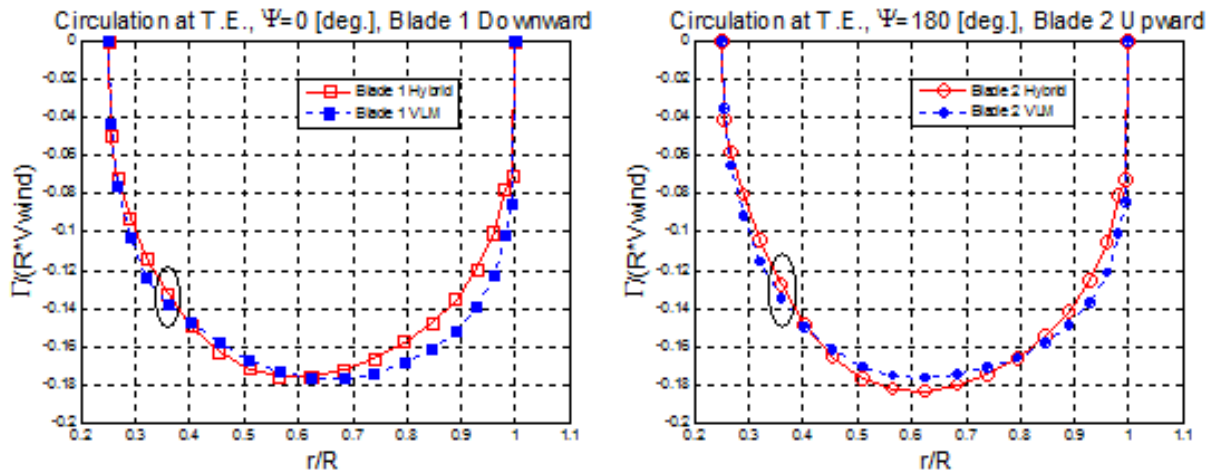


Figure 9: (a) Spanwise circulation under 10 degrees of yaw at azimuth angle 0 deg. (left); (b) at azimuth angle 180 deg. (right) (36 % section is marked for Fig. 9)

Fig. 10 shows the local circulation history at the 36 % span for 10 cycles; the position is marked by an ellipse in Fig. 9. The trailing and bound vortex filaments were carried about 6.5 rotor radii (about 65 chords) downstream of the rotor. The VLM simulation was run for a longer time (20 cycles); note that the

start-up shed vortex reached the Trefftz plane, located at 10 blade radii, allowing the solution to become periodic.

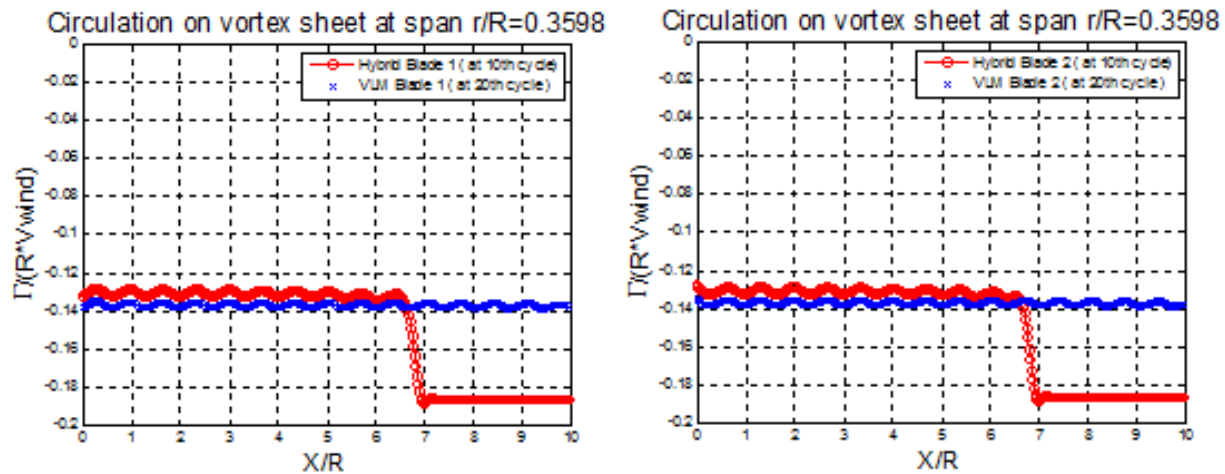


Figure 10: (a) Bound circulation history at 36 % span for blade 1 (left); (b) for blade 2 (right)

3.4 Computational cost

The computational performance was estimated using a multiple CPU system benchmark summary, updated Dec. 4, 2011. The data is partially included in the table, courtesy of Pass Mark Software Pty Ltd (see Table 2). The estimated cost of the present hybrid method is 28.4 hours (1 day and 4 hours and 24 minutes) for 10 cycles of a yawed case using the latest high speed multiple CPU system.

	System	Bench Mark score	Speed factor	Cost [sec]	Cost [day]	The system Price [USD]
The fastest	[3-Way] Intel Xeon E7- 8837@ 2.67GHz	33504	6.69	1.03e+05	1.19	NA
The second	[Quad CPU] AMD Opteron 6174	29628	5.91	1.16e+05	1.34	5119.96
The third	[Quad CPU] AMD Opteron 6168	23735	4.74	1.45e+05	1.68	3079.96
Used	[Dual CPU] Quad-Core AMD Opteron 2354	5010	1	6.87e+05	7.95	NA 578.28, June 2011

Table 2: Computational cost estimations for 10 cycles. The bench mark and price data are provided courtesy of Pass Mark Software Ltd. updated Dec. 4, 2011

To compare with full Euler or Navier-Stokes simulations, two references are reviewed. Long and Sezer-Uzol (2006) performed an Euler simulation of the NREL Phase VI rotor under yaw condition with the computational domain size 4 blade radii downstream [12]. Seven super computers were used, and the fastest computation took 1.7 days per one blade revolution using the National Center for Supercomputing Applications (NCSA) cluster. The computational speed of hybrid method is about 14.3 times faster while simulating a larger domain. F. Zahle, N. N. Sorensen and J. Johansen carried out Navier-Stokes simulations of UAE Phase VI, that included modeling of the rotor, tower and tunnel floor (2009) [13]. The mesh size is 5.57 million cells for the rotor only configuration and is 9.6 million cells for the rotor and tower configuration. The mesh size increased with a factor 1.7 when the tower is modeled. In contrast, the hybrid method can model the tower as a line of doublets (see Chattot [14]). Hence the computational cost would not significantly increase with the hybrid method with the tower model. If the factor 1.7 was tentatively applied to the Euler computation, the hybrid method would be more than 20 times faster than the full Euler computation to obtain a periodic solution.

4 Swept NREL blade under yaw

An unsteady analysis for a 10 % backward swept rotor in yawed flow is presented as an example of the new tool. The addition of sweep to the NREL blade does not change significantly the power or bending moment but is expected to improve blade static stability with respect to wind gusts as seen in earlier work [4]. The pitching moment increased, as seen in the steady simulation for all azimuth angles (see Fig. 11).

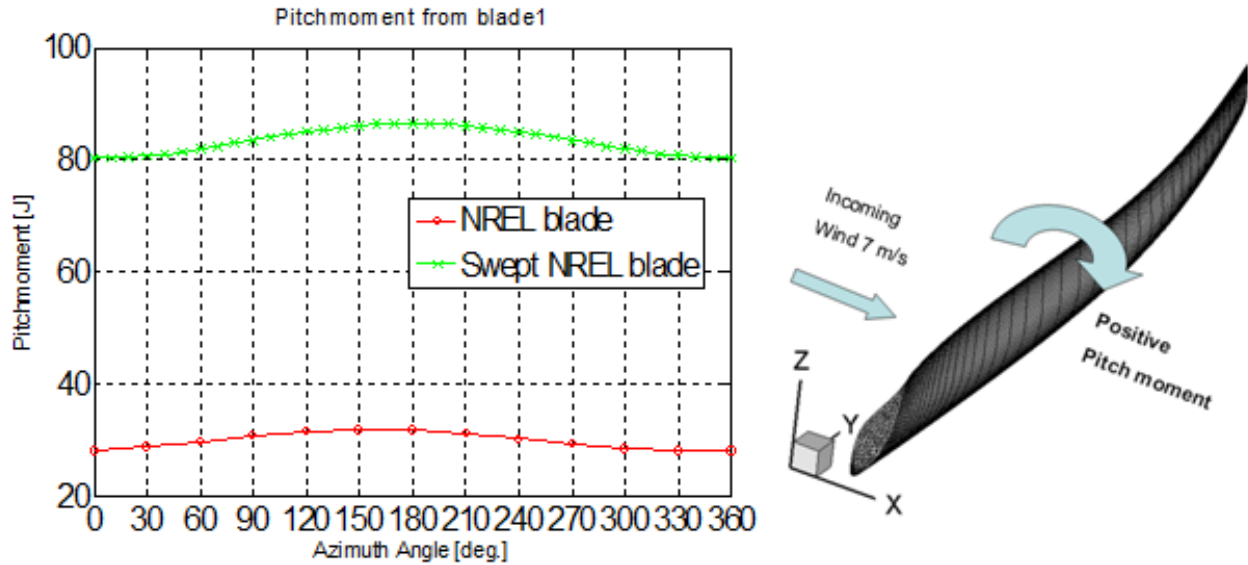


Figure 11: Pitching moment output (left) and its direction as "nose-down" (right)

Cross-flow solution contours for the v-velocity component near the trailing edge of blade 1 are presented in Fig. 12.

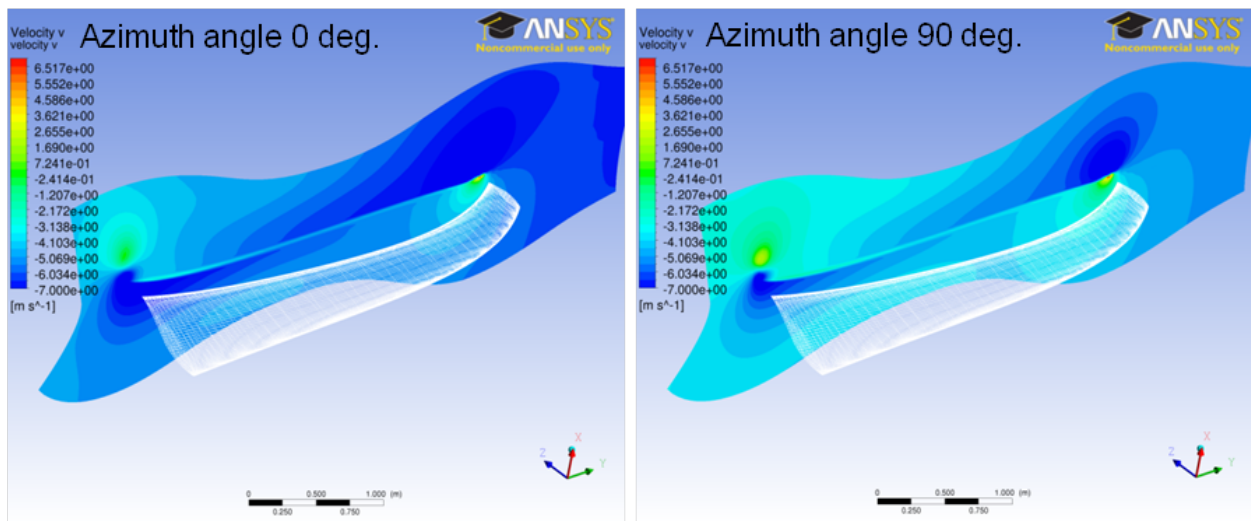


Figure 12: Cross-flow contours of the v-velocity component at 10 degrees of yaw

5 Periodic acceleration for the prescribed wake model

The "periodic acceleration" is an idea for making hybrid computations faster when a periodic solution exists. Vortex filaments are convected from the trailing edge of the blade to the Trefftz plane, and at the $U = 7 \text{ m/s}$ wind speed, it takes about 14 cycles to convect a perturbation 10 blade radii downstream. The following procedure could obtain a virtually equivalent periodic solution in a shorter time:

- 1) Calculation of the unsteady hybrid method for 1 cycle
- 2) Replication of the unsteady vortex filaments distribution of 1 cycle all the way to the Trefftz plane (as if repeated 14 times)
- 3) Calculation of another cycle
- 4) Replacement of the unsteady wake by the new cycle's replica all the way to the Trefftz plane
- 5) Repetition of the process 1) - 4) a few times until the solution becomes periodic

This procedure was tested with VLM. The virtually equivalent periodic solution was obtained in about 3 periods (cycles) within the tolerance, $10e-5$ (see Fig. 13). Fig. 14 shows the periodic acceleration converged to a periodic solution 6 times faster than impulsive unsteady calculation. Note that the first 2 time steps (the first 2 azimuth angles) of every coupling using new replica distribution in wake were not smooth and the values of the 2nd cycle were used in the Fig. 13 for the 4th coupling.

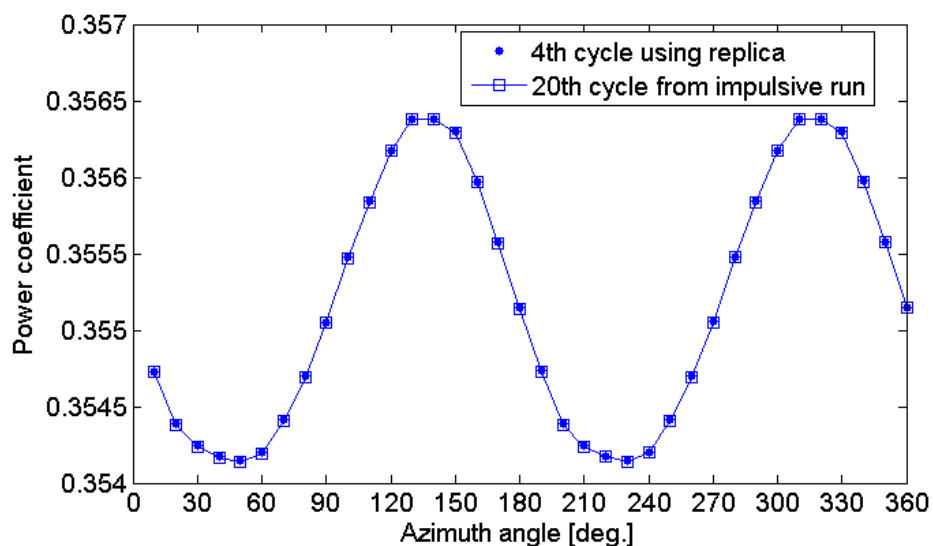


Figure 13: Power coefficient output by periodic acceleration

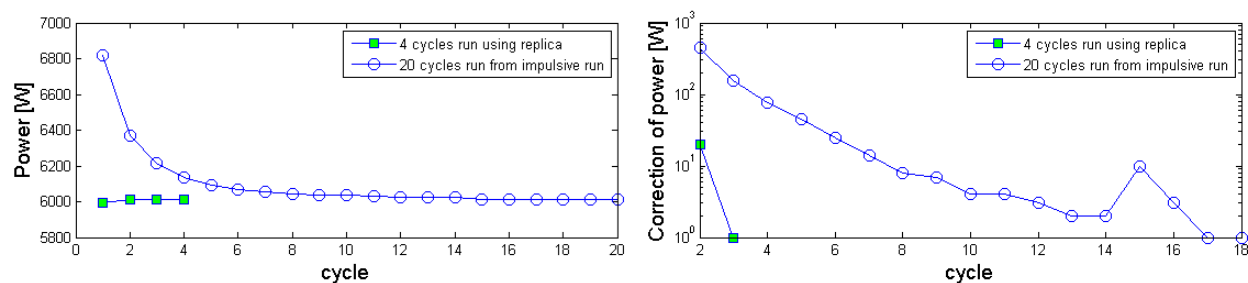


Figure 14: Power (left) and convergence (right) history

6 Conclusions

This study has shown that the unsteady coupling of Navier-Stokes solver with helicoidal vortex model successfully converged for 10 and 20 degrees of yaw in more than 15 times less computational cost than the full Euler/Navier-Stokes computations. By introducing the "periodic acceleration", the cost could decrease by another factor; the test with VLM indicates an acceleration factor of 6. For future work, the Unsteady Hybrid Navier-Stokes/Vortex Model code could be developed in two directions: one involves keeping the simplest possible model, to be used as a design/analysis tool in industry, and the other involves building higher fidelity unsteady physics in the helicoidal vortex model, to be used as a research tool, as it is expected to be a good reference code for the full unsteady Navier-Stokes computations in the next decade.

References

- [1] S. Schmitz and J. J. Chattot. A Parallelized Coupled Navier-Stokes/Vortex-Panel Solver. *ASME Journal of Solar Energy Engineering*, 127:475–487, 2005.
- [2] C. P. Butterfield, W. P. Musial, and D. A. Simms. Combined Experiment Phase I Final Report. NREL/TP-257-4655. Golden, CO., 1992.
- [3] S. Schmitz and J. J. Chattot. A coupled Navier-Stokes/Vortex-Panel solver for the numerical analysis of wind turbines. *Computers & Fluids*, 35:742–745, 2006.
- [4] K. Suzuki, S. Schmitz, and J. J. Chattot. Analysis of a Swept Wind Turbine Blade Using a Hybrid Navier-Stokes/Vortex-Panel Model. Springer-Verlag, Proceedings of the Sixth International Conference on Computational Fluid Dynamics, ICCFD6, St. Petersburg, Russia, July 12-16, 2010.
- [5] J. M. Hallissy and J. J. Chattot. Validation of a Helicoidal Vortex Model with the NREL Unsteady Aerodynamic Experiment. *Computational Fluid Dynamic Journal*, 14(3):236–245, 2005.
- [6] J. J. Chattot. Tower shadow modelization with helicoidal vortex method. *Computers & Fluids*, 37(5):499–504, 2008.
- [7] M. E. Braaten and Gopinath A. Aero-Structural Analysis of Wind Turbine Blades with Sweep and Winglets-Coupling a Vortex Line Method to ADAMS/AeroDyn. proceedings of ASME Turbo Expo 2011, June 6-10, 2011.
- [8] J. J. Chattot. Wind turbine aerodynamics: analysis and design. *Int. J. Aerodynamics*, 1, (3/4):404-444, 2008.
- [9] J. J. Chattot. Helicoidal vortex method for steady and unsteady flows. *Computers & Fluids*, 35(7):733–741, 2006.
- [10] D. A. Caughey. Implicit multigrid computation of unsteady flows past cylinders of square cross-section. *Computers & Fluids*, 30(7):939–960, 2001.
- [11] L. J. Fingersh. Unsteady Aerodynamics Experiment. *Journal of Solar Energy Engineering*, 123:267, 2001.
- [12] N. Sezer-Uzol and L. N. Long. 3-D Time-Accurate CFD Simulations of Wind Turbine Rotor Flow Fields. *AIAA Paper*, No. 2006-0394, 2006.
- [13] F. Zahle, N. N. Sørensen, and J. Johansen. Wind Turbine Rotor-Tower Interaction Using an Incompressible Overset Grid Method. *Wind Energy*, 12(6):594–619, 2009.
- [14] J. J. Chattot. Extension of a helicoidal vortex model to account for blade flexibility and tower interference. *J Solar Energy Eng.*, 128:455–460, 2006. also *AIAA Paper* 0391.